

ments are needed to clarify the identities of the quenching species and to test for the general existence of nonisomorphic intensity and lifetime quenching.

Acknowledgment. We are grateful to G. B. Schuster and B. E. Goodson for sharing their results and ideas with us, and we

are pleased to acknowledge support of this work by the National Science Foundation under Grants CHE-81-06026 and CHF 83-15177.

Registry No. TBABF₄, 429-42-5; TEABF₄, 429-06-1; TBAP, 1923-70-2; TBAPF₆, 3109-63-5; DMA, 121-69-7; pyrene, 129-00-0.

Electrocatalysis at Redox Polymer Electrodes with Separation of the Catalytic and Charge Propagation Roles. Reduction of O₂ to H₂O₂ as Catalyzed by Cobalt(II) Tetrakis(4-*N*-methylpyridyl)porphyrin

Fred C. Anson,*† Ching-Long Ni,† and Jean-Michel Saveant*‡

Contribution No. 7130 from the Division of Chemistry and Chemical Engineering, Arthur Amos Noyes Laboratories, California Institute of Technology, Pasadena, California 91125, and the Laboratoire d'Electrochimie, Universite de Paris VII, Tour 44-45, 75251 Paris, Cedex 05, France. Received December 4, 1984

Abstract: The kinetics of the reduction of O₂ by Ru(NH₃)₆²⁺ as catalyzed by cobalt(II) tetrakis(4-*N*-methylpyridyl)porphyrin are described both in homogeneous solution and when the reactants are confined to Nafion coatings on graphite electrodes. The catalytic mechanism is delineated and the factors that can control the total reduction currents at Nafion-coated electrodes are specified. A kinetic zone diagram for analyzing the behavior of catalyst-mediator-substrate systems at polymer-coated electrodes is presented and utilized in identifying the current-limiting processes. Good agreement is demonstrated between calculated and measured reduction currents at rotating disk electrodes. The experimental conditions that will yield the optimum performance of coated electrodes are discussed, and a relationship is derived for the optimal coating thickness.

Nafion coatings on electrodes offer unusually stable environments for attaching reactants to electrode surfaces.^{1,2} The attributes of such coatings were exploited in a recent study of the catalysis of the electroreduction of dioxygen by cobalt tetraphenylporphyrin incorporated in Nafion coatings on graphite electrodes.^{2d} It was necessary to incorporate a mediator redox couple such as Ru(NH₃)₆^{3+/2+} into the Nafion coating along with the cobalt porphyrin catalyst in order to carry electrons from the electrode surface to the essentially immobile catalyst sites. The resulting three-component coating (Nafion, catalyst, redox mediator) provided an effective means for the electroreduction of dioxygen, albeit at a potential determined by the formal potential of the redox mediator.^{2d} Three-component coatings allow the catalytic and charge propagation roles to be assigned to separate reactants that can be selected so as to maximize the overall rate of reaction of the substrate. It was therefore of interest to analyze the kinetics of dioxygen reduction by such a three-component electrode coating to understand how best to optimize experimental conditions in order to achieve high catalytic efficiency. This report is devoted to a kinetic analysis of a system in which cobalt(II) tetrakis(4-*N*-methylpyridyl)porphyrin was employed as the catalyst for the reduction of dioxygen to hydrogen peroxide with Ru(NH₃)₆^{3+/2+} as the redox mediator. The water solubility of the catalyst allowed the kinetics to be measured in homogeneous solution as well as with the catalyst and mediator incorporated in Nafion coatings on rotating graphite disk electrodes. In both cases, the reaction appears to follow a "preactivation" mechanism in which only a preformed dioxygen-catalyst adduct is able to accept electrons from the redox mediator at a high rate. The reaction scheme thus involves a combination of "chemical catalysis" (formation of the adduct) and "redox catalysis" (outer-sphere reduction of the adduct) in the senses defined and

analyzed by Andrieux et al.³ Such preactivation mechanisms seem likely to be among the most frequently encountered in practical applications of electrodes coated with redox polymers. For example, the utilization of biological catalysts such as metalloenzymes as electrocatalysts⁴ is likely to involve preactivation mechanisms and may often require separate redox mediators to provide rapid charge propagation throughout electrode coatings. For these reasons, we have analyzed the kinetic behavior of this first example of a preactivation catalytic mechanism at a redox polymer electrode in some detail and present our results in this report.

Experimental Section

Materials. Ru(NH₃)₆Cl₃ (Strem Chemical Co.) was purified according to the procedure of Pladziewicz et al.⁵ Standard solutions of Ru(NH₃)₆³⁺ were prepared by dissolving accurately weighed samples of Ru(NH₃)₆Cl₃ in 0.1 M lithium acetate-acetic acid buffer (pH 4.5). The

- (1) (a) Rubinstein, I.; Bard, A. J. *J. Am. Chem. Soc.* **1980**, *102*, 6641. (b) Rubinstein, I.; Bard, A. J. *J. Am. Chem. Soc.* **1981**, *103*, 5007. (c) Henning, T. P.; White, H. S.; Bard, A. J. *J. Am. Chem. Soc.* **1981**, *103*, 3937. (d) White, H. W.; Leddy, J.; Bard, A. J. *J. Am. Chem. Soc.* **1982**, *104*, 4811. (e) Martin, C. R.; Rubinstein, I.; Bard, A. J. *J. Am. Chem. Soc.* **1982**, *104*, 4817. (f) Krishnan, M.; Zhang, X.; Bard, A. J. *J. Am. Chem. Soc.* **1984**, *106*, 7371. (2) (a) Buttry, D. A.; Anson, F. C. *J. Electroanal. Chem.* **1981**, *130*, 333. (b) Buttry, D. A.; Anson, F. C. *J. Am. Chem. Soc.* **1982**, *104*, 4824. (c) Buttry, D. A.; Anson, F. C. *J. Am. Chem. Soc.* **1983**, *105*, 685. (d) Buttry, D. A.; Anson, F. C. *J. Am. Chem. Soc.* **1984**, *106*, 59. (e) Tsou, Y.-M.; Anson, F. C. *J. Electrochem. Soc.* **1984**, *131*, 595. (f) Buttry, D. A.; Saveant, J.-M.; Anson, F. C. *J. Phys. Chem.* **1984**, *88*, 3086. (3) (a) Andrieux, C. P.; Dumas-Bouchiat, J. M.; Saveant, J.-M. *J. Electroanal. Chem.* **1978**, *87*, 39. (b) *J. Electroanal. Chem.* **1978**, *87*, 55. (c) *J. Electroanal. Chem.* **1978**, *88*, 43. (d) *J. Electroanal. Chem.* **1980**, *113*, 1. (e) *J. Electroanal. Chem.* **1980**, *113*, 19. (4) Lee, C.-W.; Gray, H. B.; Maimstrom, B. G.; Anson, F. C. *J. Electroanal. Chem.* **1984**, *172*, 289. (5) Pladziewicz, J. R.; Meyer, T. J.; Broomhead, J. A.; Taube, H. *Inorg. Chem.* **1973**, *12*, 639.

* Arthur Amos Noyes Laboratories.

† Laboratoire d'Electrochimie.

resulting solution was deaerated with argon and reduced with zinc amalgam for 30 min to produce $\text{Ru}(\text{NH}_3)_6^{2+}$. Cobalt(II) was introduced into tetrakis(4-*N*-methylpyridyl)porphine *p*-toluenesulfonate (Mid-Century Chemical Co.) under an Ar atmosphere according to the published procedure⁶ and the product precipitated by addition of excess NH_4PF_6 . A gas mixture containing 2.1% O_2 in N_2 was obtained from Matheson.

Soluble Nafion (equiv wt = 970) was available as a 5.2 wt % solution obtained some time ago from E. I. DuPont de Nemours and Co. Similar material is presently commercially available from C & G Processing, Rockland, DE. Basal plane pyrolytic graphite (Union Carbide Co.) was cut and mounted on rotatable shafts to produce rotating disk electrodes as previously described.⁷

Apparatus and Procedures. Electrochemical measurements were conducted with appropriate combinations of PAR (EG&G Instrument Co.) instruments. Rotating disk electrodes were rotated with an ASR2 rotator and ASR controller from Pine Instrument Co. Absorption spectra were obtained with a Hewlett-Packard Model 8450A spectrophotometer and HP 7225A plotter.

Electrodes were coated with Nafion by transferring a few microliters of a 5.1 mM solution (prepared by diluting the 5.2 wt % stock solution with isopropyl alcohol) to a freshly cleaved electrode surface and allowing the solvent to evaporate. Coatings containing cobalt(II) tetrakis(4-*N*-methylpyridyl)porphyrin (CoTMPyP) were applied in a similar fashion by using the homogeneous solution prepared by mixing the Nafion stock solution in isopropyl alcohol with an equal volume of an aqueous solution of CoTMPyP. The resulting solution appeared homogeneous and no precipitate formed upon long standing. The absorption spectra of CoTMPyP dissolved in H_2O or in a 1:1 mixture of H_2O and isopropanol containing 0.5 wt % Nafion are almost identical. Both the spectrum of the Nafion-CoTMPyP mixture and the catalytic activity of coatings prepared from it remained constant for periods of several months.

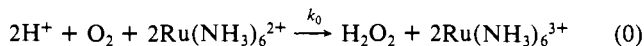
$\text{Ru}(\text{NH}_3)_6^{3+}$ was incorporated into both types of coatings by soaking them in solutions of the complex. The quantity of CoTMPyP and $\text{Ru}(\text{NH}_3)_6^{3+}$ incorporated in the coatings was determined coulometrically as described in detail in the Results section.

Potentials were measured and are reported with respect to a saturated calomel reference electrode (SCE).

The rate of the reaction between O_2 and $\text{Ru}(\text{NH}_3)_6^{2+}$ was followed under pseudo-first-order conditions by means of a graphite rotating disk electrode. The electrode was rotated at 3600 rpm in an air-saturated solution which resulted in complete mixing of the solution within a few seconds. The electrode potential was maintained at 0.5 V where the oxidation of $\text{Ru}(\text{NH}_3)_6^{2+}$ to $\text{Ru}(\text{NH}_3)_6^{3+}$ produced a limiting current proportional to the time-dependent concentration of $\text{Ru}(\text{NH}_3)_6^{2+}$. There were no significant contributions to the current from O_2 , H_2O_2 , or CoTMPyP at this potential and the kinetic runs were short enough to ensure that negligible quantities of $\text{Ru}(\text{NH}_3)_6^{2+}$ were consumed by the electrode reaction or by the H_2O_2 that was the product of the reduction of O_2 . Kinetic runs were initiated by injecting an aliquot of $\text{Ru}(\text{NH}_3)_6^{2+}$ into the air-saturated reaction solution containing the rotating disk electrode and the desired concentration of CoTMPyP. Air from a gas dispersion tube was passed through the solutions throughout each run to ensure that the concentration of O_2 remained constant. The tube was positioned to ensure that the limiting currents were unaffected by the continuous flow of gas bubbles.

Results

Uncatalyzed Reduction of O_2 by $\text{Ru}(\text{NH}_3)_6^{2+}$. Curve 1 in Figure 1A traces the current for the oxidation of $\text{Ru}(\text{NH}_3)_6^{2+}$ at a rotating disk electrode in a solution saturated with air. The magnitude of the current produces a continuous measure of the concentration of $\text{Ru}(\text{NH}_3)_6^{2+}$ and the linear plot of log current vs. time in curve 1 of Figure 1B confirms that the rate of the uncatalyzed reduction of O_2 by $\text{Ru}(\text{NH}_3)_6^{2+}$ according to eq 0 is first-order in $\text{Ru}(\text{NH}_3)_6^{2+}$.⁸ The pseudo-first-order rate constant obtained from



the slope of line 1 in Figure 1B is $4.4 \times 10^{-2} \text{ s}^{-1}$. Since reaction 0 is also known to be first-order in O_2 ,⁸ this rate constant corresponds to a second-order constant of $79 \text{ M}^{-1} \text{ s}^{-1}$ for an O_2 concentration of 0.28 mM in an air-saturated solution at 22 °C.⁵

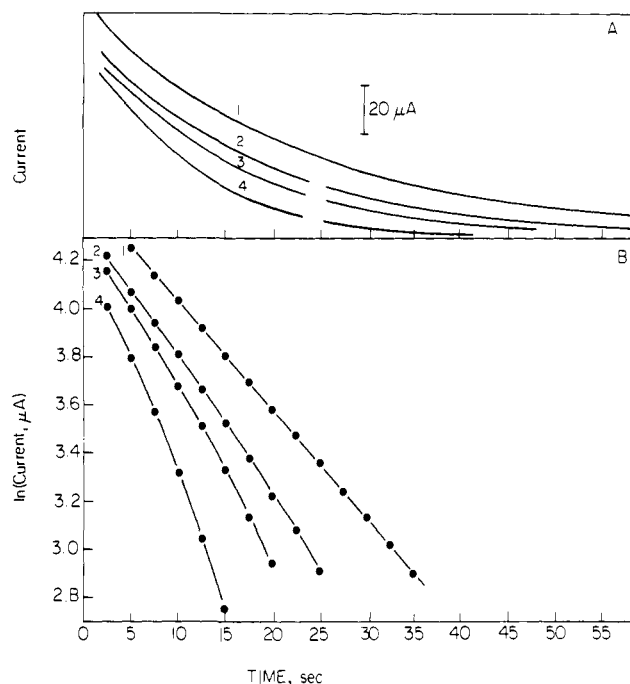
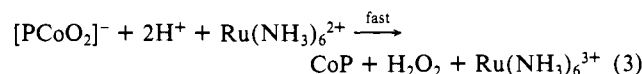
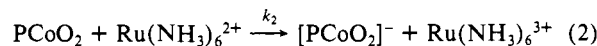
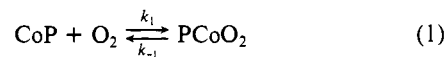


Figure 1. (A) Current vs. time plots for the oxidation of $\text{Ru}(\text{NH}_3)_6^{2+}$ by O_2 . Rotating disk electrode was held at +0.5 V (vs. SCE) and rotated at 3600 rpm. Initial concentration of $\text{Ru}(\text{NH}_3)_6^{2+}$: 500 μM . $[\text{CoP}] = 0$ (1); 5.0 (2); 9.7 (3); 19 μM (4). Supporting electrolyte: $\text{CH}_3\text{COO-Li-CH}_3\text{COOH}$, pH = 4.5, $\mu = 0.1 \text{ M}$. (B) Corresponding plots of $\ln(\text{current})$ vs. time. Curves 2, 3, and 4 are not linear. See the text for details.

This value of k_0 is in reasonable agreement with the $63 \text{ M}^{-1} \text{ s}^{-1}$ value reported by Stanbury et al.,⁸ indicating that the rotating disk procedure is a reliable method for following the kinetics of the reaction.

Catalyzed Reduction of O_2 . Addition of small quantities of CoTMPyP ($\equiv \text{CoP}$ hereafter) to solutions of $\text{Ru}(\text{NH}_3)_6^{2+}$ and O_2 enhances the rate of reduction of O_2 significantly. Curves 2, 3, and 4 in Figure 1A show the effect of increasing quantities of the CoP catalyst. Curves 2–4 yield nonlinear plots of $\ln(\text{current})$ vs. time (Figure 1B), indicating that the catalytic mechanism involves more than a simple pre-equilibrium between CoP and O_2 to form a more rapidly reduced adduct. (Separate experiments conducted in the absence of O_2 demonstrated that further reduction of the H_2O_2 produced in the primary reaction proceeds at a negligible rate both in the absence and the presence of CoP.)

The kinetics were therefore assumed to be controlled by the formation of a more reactive CoP-O_2 adduct whose concentration attained a small, steady-state value. The steps involved in the catalyzed reduction are believed to be those given in reactions 1–3.¹⁰



The steady-state assumption for $[\text{CoPO}_2]$ yields

$$[\text{PCoO}_2] = \frac{k_1[\text{CoP}][\text{O}_2]}{k_2[\text{Ru}^{II}] + k_{-1}} \quad (4)$$

(10) An alternative mechanism in which the porphyrin catalyst acts to stabilize O_2^- generated in an outer-sphere reaction between O_2 and $\text{Ru}(\text{NH}_3)_6^{2+}$ could be ruled out both by the lack of inhibition by $\text{Ru}(\text{NH}_3)_6^{3+}$ and the observation that the catalyzed reaction proceeded much more rapidly than the rate with which $\text{Ru}(\text{NH}_3)_6^{2+}$ reduces O_2 to O_2^- .⁸

(6) Hambricht, P.; Fleischer, E. B. *Inorg. Chem.* **1970**, *9*, 1757.

(7) Oyama, N.; Anson, F. C. *Anal. Chem.* **1980**, *52*, 1192.

(8) Stanbury, D. M.; Haas, O.; Taube, H. *Inorg. Chem.* **1980**, *19*, 518.

(9) "Solubilities of Inorganic and Metallorganic Compounds"; Linke, W. F., 4th ed.; American Chemical Society: Washington, D.C., 1965; Vol. 11.

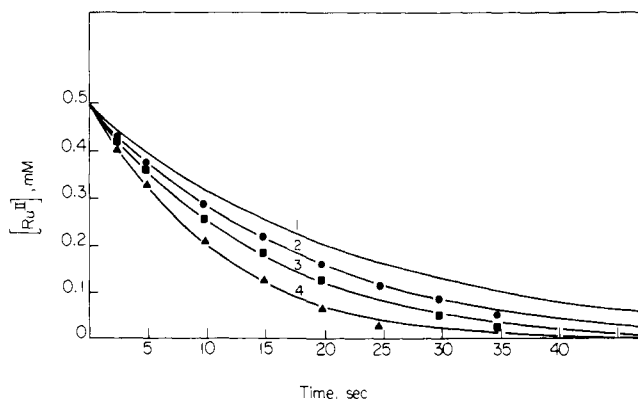


Figure 2. Comparison of calculated (curves) and experimental (points) values of $[\text{Ru}(\text{NH}_3)_6^{2+}]$ during its oxidation by O_2 . The curves were generated by numerical integration of eq 6 with the constants $k_1 = 3.6 \times 10^3 \text{ M}^{-1} \text{ s}^{-1}$ and $k_2/k_{-1} = 1.7 \times 10^3 \text{ M}^{-1}$. The points were obtained from the corresponding curves of Figure 1A.

where $\text{Ru}^{\text{II}} \equiv \text{Ru}(\text{NH}_3)_6^{2+}$. The rate of the catalyzed reduction of O_2 is then given by

$$-2 \left(\frac{d\text{O}_2}{dt} \right)_{\text{cat}} = - \left(\frac{d\text{Ru}^{\text{II}}}{dt} \right)_{\text{cat}} = \frac{2k_2k_1[\text{CoP}][\text{O}_2][\text{Ru}^{\text{II}}]}{k_2[\text{Ru}^{\text{II}}] + k_{-1}} \quad (5)$$

The overall, observed reduction rate is given by eq 6.

$$-2 \left(\frac{d\text{O}_2}{dt} \right) = - \left(\frac{d[\text{Ru}^{\text{II}}]}{dt} \right) = \frac{2k_2k_1[\text{CoP}][\text{O}_2][\text{Ru}^{\text{II}}]}{k_2[\text{Ru}^{\text{II}}] + k_{-1}} + 2k_0[\text{O}_2][\text{Ru}^{\text{II}}] \quad (6)$$

The second term on the rhs of eq 6 could be evaluated at every point of an experiment because k_0 and $[\text{O}_2]$ were known constants and $[\text{Ru}^{\text{II}}]$ was available from the magnitude of the oxidation current at the rotating disk electrode. Equation 6 was integrated numerically¹¹ to calculate values of $[\text{Ru}^{\text{II}}]$ vs. time for various values of the unknown rate constants.

Figure 2 compares plots of the calculated values of $[\text{Ru}^{\text{II}}]$ with the experimental data points for three kinetic runs. The values of $2k_1[\text{Co}^{\text{II}}][\text{O}_2]$ and $k_1/(2k_2k_1[\text{Co}^{\text{II}}][\text{O}_2])$ were varied to obtain the best agreement between the calculated curves and the data points. The best fit, shown in Figure 2, resulted for $k_1 = 3.6 \times 10^3 \text{ M}^{-1} \text{ s}^{-1}$ and $k_2/k_{-1} = 1.7 \times 10^3 \text{ M}^{-1}$.

At concentrations of Ru^{II} where $k_2[\text{Ru}^{\text{II}}] \ll k_{-1}$, the formation

Table I. Coulometric Assay of $\text{Co}^{\text{III}}\text{P}$ in Nafion Coatings

| comp of deposited coating | | coulometric assay |
|---|--|--|
| $10^7 \Gamma_{\text{NF}}^a$ mol cm^{-2} | $10^9 \Gamma_{\text{Co}^{\text{III}}\text{P}}^b$ mol cm^{-2} | $10^9 \Gamma_{\text{Co}^{\text{III}}\text{P}}^c$ mol cm^{-2} |
| 1.5 | 2.5 | 1.9 |
| 1.5 | 3.7 | 3.0 |
| 0.9 | 1.5 | 1.1 |

^a Sulfonate groups in the aliquot of Nafion- $\text{Co}^{\text{III}}\text{P}$ solution used to coat the electrode. ^b Quantity of $\text{Co}^{\text{III}}\text{P}$ in the aliquot of Nafion- $\text{Co}^{\text{III}}\text{P}$ solution used to coat the electrode. ^c Quantity of $\text{Co}^{\text{III}}\text{P}$ in the coatings as measured coulometrically (see text).

of the CoP-O_2 adduct can be regarded as a rapid preequilibrium step and eq 6 can be integrated to give eq 7 where $[\text{Ru}^{\text{II}}]_0$ is the

$$\ln [\text{Ru}^{\text{II}}] = \ln [\text{Ru}^{\text{II}}]_0 - k_{\text{obsd}} t \quad (7)$$

initial concentrations of $\text{Ru}(\text{NH}_3)_6^{2+}$ and $k_{\text{obsd}} = 2[\text{O}_2](((k_1k_2[\text{CoP}])/k_{-1}) + k_0)$. Figure 3A contains plots of $\ln(\text{current})$ vs. t at low concentrations of $[\text{Ru}^{\text{II}}]$ that exhibit the linearity expected from eq 7. The slopes of the lines and the known values of k_0 and $[\text{O}_2]$ were used to obtain values of $k_1k_2[\text{CoP}]$ that yielded the linear plots in Figure 3B, showing that the reaction rate is first-order with respect to the CoP catalyst. The slope and intercept of the line in Figure 3B correspond to $k_1k_2/k_{-1} = K_1k_2 = 1.3 \times 10^7 \text{ M}^{-2} \text{ s}^{-1}$ and $k_0 = 77 \text{ M}^{-1} \text{ s}^{-1}$, respectively. This value of K_1k_2 compares favorably with the value, $0.6 \times 10^7 \text{ M}^{-2} \text{ s}^{-1}$, obtained by fitting the curves in Figure 2, and the value of k_0 is close to the value measured independently.

At sufficiently high concentrations of $\text{Ru}(\text{NH}_3)_6^{2+}$ where $k_2[\text{Ru}^{\text{II}}] \gg k_{-1}$, the rate of the CoP -catalyzed reduction of O_2 would be expected to reach a limiting value given by $k_1[\text{CoP}][\text{O}_2]$. We were not able to observe this condition experimentally because the uncatalyzed reaction rate became dominant at the high concentrations of $\text{Ru}(\text{NH}_3)_6^{2+}$ necessary to reach the saturation rate of the catalyzed reaction pathway.

Voltammetry of CoP when Adsorbed on the Graphite Surface or Incorporated in Nafion Coatings. CoP is adsorbed on the surfaces of pyrolytic graphite electrodes strongly and irreversibly so that a voltammetric response remains when the electrodes are transferred to pure supporting electrolyte solutions. Curve A in Figure 4 shows the response obtained from ca. $3 \times 10^{-11} \text{ mol cm}^{-2}$ of CoP adsorbed on a graphite electrode. Adsorption of the porphyrin on the surface leads to a large increase in the background current apparently because of an increase in the capacitive charging current. However, the responses arising from CoP and the quinone-hydroquinone functions on the graphite surface remain evident at 0.48 and 0.1 V, respectively. The $\text{Co}^{\text{III/II}}$ response

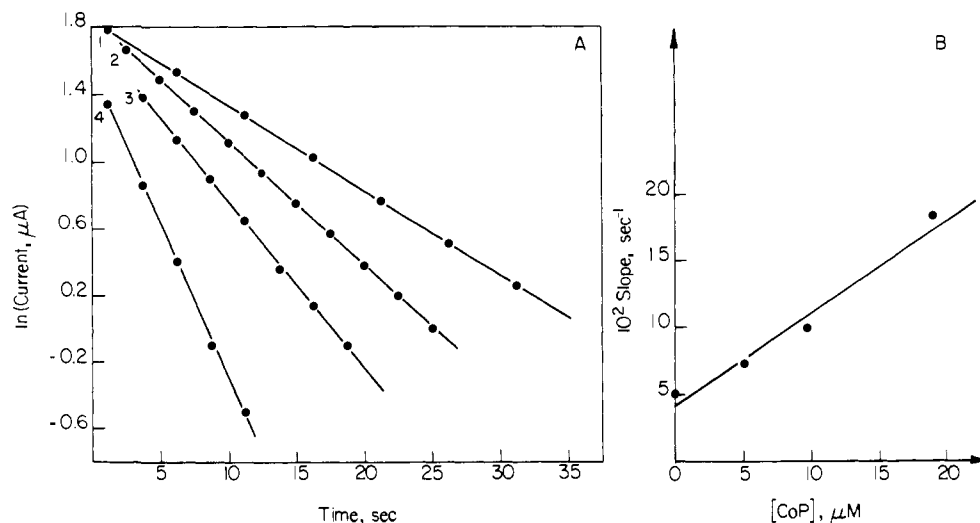


Figure 3. (A) Kinetic plots of the oxidation of low concentrations of $\text{Ru}(\text{NH}_3)_6^{2+}$ by O_2 . Initial $[\text{Ru}(\text{NH}_3)_6^{2+}] = 20 \mu\text{M}$. Other conditions as in Figure 2. (B) Slopes of the lines in A vs. $[\text{CoP}]$.

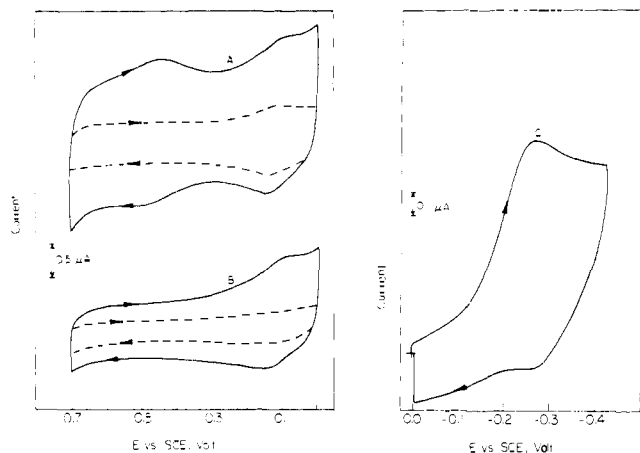


Figure 4. Cyclic voltammograms of CoP and a $\text{Ru}(\text{NH}_3)_6^{3+}$ -CoP mixture at basal plane graphite electrodes. (A) Bare graphite electrode on which ca. 3×10^{-11} mol cm^{-2} CoP had been adsorbed. The dashed line is the background response of the bare graphite electrode. Scan rate: 100 mV s^{-1} . (B) Electrode coated with 1.5×10^{-7} mol cm^{-2} Nafion in which 3.7×10^{-9} mol cm^{-2} CoP was incorporated. The dashed line is the background response of the electrode coated only with 1.5×10^{-7} mol cm^{-2} Nafion. Scan rate: 100 mV s^{-1} . (C) Cyclic voltammogram of $\text{Ru}(\text{NH}_3)_6^{3+}$ incorporated in a 1.5×10^{-7} mol cm^{-2} Nafion coating which also contains 2.5×10^{-9} mol cm^{-2} CoP. Scan rate: 5 mV s^{-1} . Supporting electrolyte: 0.1 M acetate buffer (pH 4.5) saturated with Ar. To record curve C, 2×10^{-8} M $\text{Ru}(\text{NH}_3)_6^{3+}$ was also present.

from adsorbed CoP appears at a considerably more positive value than the formal potential of the porphyrin in aqueous acid (0.17 V),¹² showing that adsorption on the graphite surface stabilizes Co^{II} P much more than Co^{III} P, possibly as a result of axial coordination of unsaturated ligand groups present on the surface of the graphite.

Curve B in Figure 4 resulted when the electrode was coated with a mixture of 1.5×10^{-7} mol cm^{-2} of Nafion and 3.7×10^{-9} mol cm^{-2} of CoP. There is essentially no faradaic response from the electrode coated with the CoP-Nafion mixture except for the background current associated with the graphite surface. (The reason for the absence of the quinone-hydroquinone waves in the dashed curve of Figure 4B is not clear.) The lack of response is the result of the very small diffusion coefficients of metalloporphyrins in Nafion coatings^{2d} that prevent them from moving to the electrode surface to react at a significant rate. The high cationic charge of CoP presumably makes its rate of diffusion through the polyanionic Nafion coating even smaller than that of uncharged porphyrins. To realize the catalytic activity of complexes that are immobilized in electronically insulating electrode coatings, it is convenient to introduce into the coating a rapidly diffusing redox couple that serves to shuttle electrons between the electrode and the catalyst sites.^{2d} The $\text{Ru}(\text{NH}_3)_6^{3+/2+}$ couple is suitable for this purpose, and Figure 4C shows the cyclic voltammogram response obtained when both $\text{Ru}(\text{NH}_3)_6^{3+}$ and Co^{III} P are incorporated in a Nafion coating. (The Co^{III} P was prepared by electrolysis of a solution of Co^{II} P at 0.6 V by using a graphite plate electrode.) The cathodic peak at -0.27 V involves the direct reduction of Co^{III} P by its reaction with $\text{Ru}(\text{NH}_3)_6^{2+}$. The anodic peak current is much smaller because only the oxidation of $\text{Ru}(\text{NH}_3)_6^{2+}$ contributes to it.

To measure the quantity of reducible Co^{III} P present in the coating, a pair of coulometric experiments was performed: The potential of an electrode coating containing $\text{Ru}(\text{NH}_3)_6^{3+}$ and Co^{III} P was swept slowly (2 mV s^{-1}) from 0 to -0.45 V and maintained at this value until the current had decayed to background levels. The total cathodic charge that passed (after correction for background charging) corresponded to the sum of the electroactive Co^{III} P and $\text{Ru}(\text{NH}_3)_6^{3+}$ present in the coating

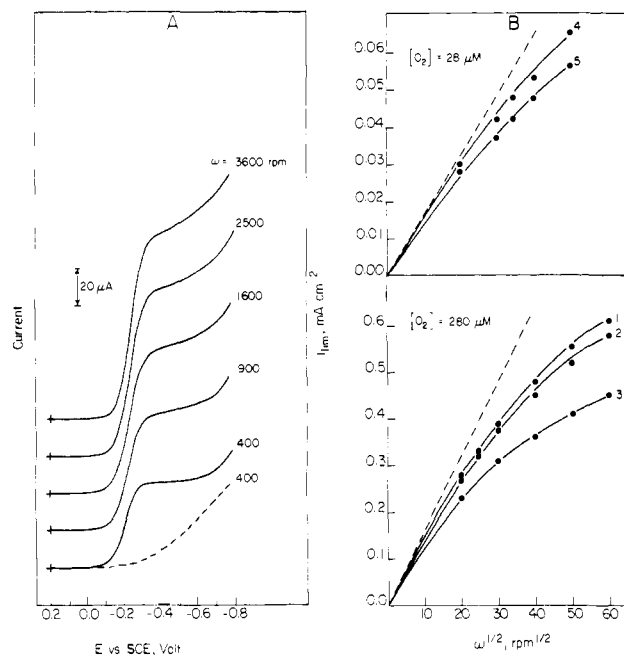


Figure 5. (A) Current-potential curves for the reduction of dioxygen at a rotating disk graphite electrode coated with Nafion in which 2.5×10^{-9} mol cm^{-2} CoP and 1.9×10^{-8} mol cm^{-2} $\text{Ru}(\text{NH}_3)_6^{3+}$ were incorporated. The dashed line is the response that resulted when the $\text{Ru}(\text{NH}_3)_6^{3+}$ was omitted. Supporting electrolyte: 0.1 M acetate buffer (pH 4.5) saturated with air. Scan rate: 2 mV s^{-1} . (B) Levich plots of the limiting O_2 reduction for curves such as those in part A vs. the (electrode rotation rate)^{1/2}. Coating compositions are as follows: curve 1, $10^9 \Gamma_{\text{Co}}$ (mol cm^{-2}), $10^8 \Gamma_{\text{Ru}}$ (mol cm^{-2}); 1 and 4, 3, 1.8; 2 and 5, 1.9, 1.9; 3, 1.1, 1.2. The dashed lines are the calculated responses for the diffusion-convection limited, two-electron reduction of O_2 . Other experimental conditions as in part A.

plus a very small contribution from the 2×10^{-7} M $\text{Ru}(\text{NH}_3)_6^{3+}$ that was added to the supporting electrolyte solution to suppress the loss of $\text{Ru}(\text{NH}_3)_6^{3+}$ from the coating. Next, the potential was maintained at 0 V until all the $\text{Ru}(\text{NH}_3)_6^{2+}$ that had been generated at -0.45 V was reoxidized to $\text{Ru}(\text{NH}_3)_6^{3+}$ without reoxidation of any of the Co^{II} P. Finally, the initial coulometric measurement was repeated to obtain a faradaic charge proportional to the total $\text{Ru}(\text{NH}_3)_6^{3+}$ in the coating. The difference between the two faradaic charges provided a measure of the quantity of the CoP within the coating that was accessible for reaction with the $\text{Ru}(\text{NH}_3)_6^{2+}$ redox mediator. Table I contains a set of measurements showing that about 80% of the CoP initially deposited on the electrode surface remains there and is available for reaction with $\text{Ru}(\text{NH}_3)_6^{2+}$. The missing CoP is not lost from the coating by dissolving in the solution because coatings deposited on transparent glass slides instead of graphite electrodes were shown by spectrophotometric measurements to retain all the CoP in the original coating even after long exposure to the supporting electrolyte solution. Similar electrochemical inaccessibility of reactants incorporated in Nafion coatings was also observed in a previous study in which $\text{Ru}(\text{bpy})_3^{2+}$ (bpy = 2,2'-bipyridine) was dissolved in the Nafion solution used to coat electrodes.^{1c}

Reduction of O_2 at Coated Electrodes. To observe the catalyzed reduction of O_2 without contributions to the currents from the $\text{Ru}(\text{NH}_3)_6^{3+}$ incorporated in the electrode coatings, steady-state measurements were made with rotating disk electrodes coated with the Nafion-CoP- $\text{Ru}(\text{NH}_3)_6^{3+}$ mixture. Figure 5A contains a set of current-potential curves for O_2 reduction at such electrodes in an air-saturated solution. The dashed curve shows the direct reduction of O_2 at the electrode surface that is obtained when no $\text{Ru}(\text{NH}_3)_6^{3+}$ is present in the coating. No clear current plateau appears in this case because the reduction of dioxygen merges with the background current for reduction of protons under these conditions. To avoid the slow loss of $\text{Ru}(\text{NH}_3)_6^{3+}$ from coatings in pure supporting electrolyte, $1-2 \times 10^{-6}$ M $\text{Ru}(\text{NH}_3)_6^{3+}$ was usually added. This tactic was (surprisingly) effective in main-

(11) Kreyszig, E. "Advanced Engineering Mathematics", 4th ed.; Wiley: New York, 1979; p 787.

(12) Rohrbach, D. F.; Deutsch, E.; Heineman, W. R.; Pasternak, R. F. *Inorg. Chem.* 1977, 16, 2650.

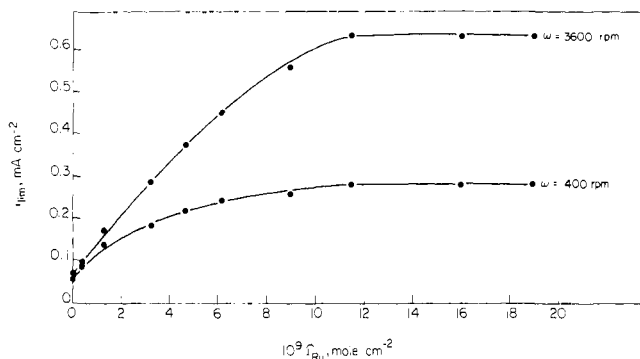


Figure 6. Limiting O_2 reduction currents at an electrode coated with Nafion-CoP-Ru(NH $_3$) $_6^{3+}$ as a function of the quantity of Ru(NH $_3$) $_6^{3+}$ in the coating. $\Gamma_{Co} = 3.7 \times 10^{-9}$ mol cm $^{-2}$. Supporting electrolyte: 0.1 M acetate buffer (pH 4.5) saturated with air and also containing 2×10^{-6} M Ru(NH $_3$) $_6^{3+}$.

taining essentially constant levels of Ru(NH $_3$) $_6^{3+}$ in coatings over a wide range of values. Fortunately the currents resulting from the reduction of such small concentrations of Ru(NH $_3$) $_6^{3+}$ were negligibly small compared to those for the reduction of O_2 .

It is important to note that the curves in Figure 5A show increasing contributions from the direct reduction of O_2 at the electrode as the electrode rotation rate increases. This is the behavior expected when the catalyzed reduction proceeds at too low a rate to consume all the O_2 that is diffusing through the coating before it reaches the electrode surface. In such cases, a second, direct reduction wave appears that is useful diagnostically in assigning kinetic mechanisms at polymer-coated electrodes.¹³

Levich plots¹⁴ of the limiting currents vs. $\omega^{1/2}$ for curves such as those in Figure 5A are shown in Figure 5B for two concentrations of O_2 (estimated from the composition of the gas mixtures assuming Henry's law to apply). The measured currents fall below those calculated for the pure diffusion-convection-controlled reduction of O_2 to H_2O_2 (dashed lines in Figure 5B). Such behavior signals that the current is limited by a process other than the supply of O_2 reaching the surface of the coated electrode. The kinetics of the electron-transfer reactions proceeding within the coatings and the transport of O_2 and/or Ru(NH $_3$) $_6^{3+/2+}$ through the coating are all possible current-limiting processes.

At a fixed electrode rotation rate, ω , with a constant quantity of CoP in the coating, the magnitude of the limiting O_2 reduction currents depended on the quantity of Ru(NH $_3$) $_6^{3+}$ in the coatings as shown in Figure 6. With sufficient quantities of incorporated Ru(NH $_3$) $_6^{3+}$, the currents became independent of the amount of Ru(NH $_3$) $_6^{3+}$ present while remaining well below the calculated Levich currents for the two-electron reduction of O_2 . Under these conditions, the rate of reaction 2 (proceeding within the coating) is so large that only reaction 1 needs to be considered as a possible current-limiting process. At the lower values of Γ_{Ru} where the measured currents become dependent on Γ_{Ru} (Figure 6), the kinetics of reaction 2 must also be considered. We will consider first the data obtained for values of Γ_{Ru} on the plateaus of the curves in Figure 6.

Kinetic Analysis. In analyzing the interplay of the various kinetic and transport processes that determine the measured plateau currents at electrodes coated with redox polymers, it is instructive to utilize kinetic zone diagrams.¹⁵ Theoretical analyses and zone diagrams for CE mechanisms (i.e., a slow chemical step preceding electron transfer) are available for cases involving homogeneous catalysis¹⁶ as well as the catalysis of electrode processes proceeding at uncoated¹⁵ and at polymer-coated electrodes.¹⁷ Zone diagrams presented previously for the case of

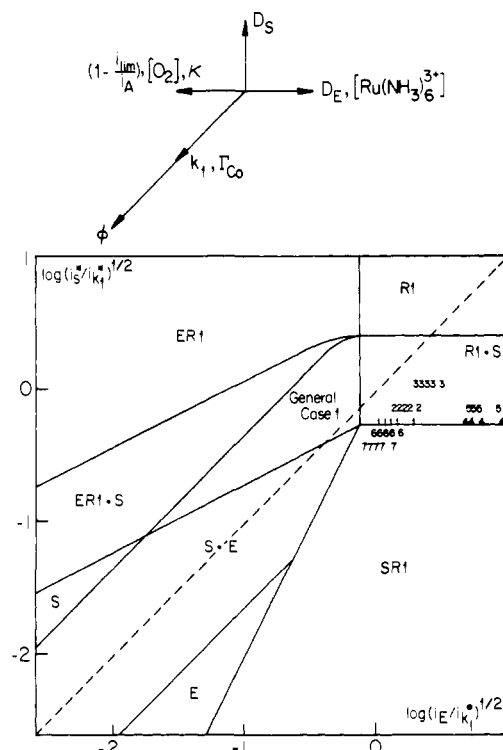


Figure 7. Kinetic zone diagram for a preactivation mechanism as adapted from ref 18 for application to the mechanism of reactions 1–3. The zones labeled ER1, R1, etc., specify the conditions where the various possible current-limiting processes become dominant.³ The vectorial diagram at the top gives the magnitude and direction of the movement within the diagram that results when the indicated experimental parameters are increased. The data points entered as small numbers in the diagram correspond to the experiment numbers in Table III. Each point represents a different electrode rotation rate.

rotating disk voltammetry¹⁷ are not applicable to the present case because they were derived for simpler mechanisms in which the catalyst is also the reactant responsible for the transport of electrons between the electrode and the substrate. However, a recent treatment of “preactivation” mechanisms at redox polymer films¹⁸ was adaptable for use with the present system. Reaction 1 amounts to “preactivation” of the substrate (O_2) prior to its reduction in the same sense that the term is employed in ref 18 except that reaction 1 is a second- instead of a first-order reaction. However, it was possible to operate under pseudo-first-order conditions so that this difference presented no problem. The treatment of ref 18 also does not encompass the possibility of a parallel unactivated reaction pathway, e.g., direct reduction of O_2 by Ru(NH $_3$) $_6^{2+}$. However, by operating under conditions where this pathway made negligible contributions to the measured currents, this possible complication was avoided. The relevant zone diagram for the mechanism embodied in reactions 1–3 under conditions where reaction 1 is rate-limiting (e.g., at high concentrations of Ru(NH $_3$) $_6^{3+}$) is shown in Figure 7. The letters R, E, and S denote the various combinations of kinetic, electron-transport, and substrate-transport processes, respectively, that can limit the measured currents.¹⁸

To proceed with an analysis of our data on the basis of the diagram of Figure 7, it is necessary to evaluate three experimental parameters: i_s^* , i_E , and i_k^* . i_s , defined by eq 8, is the current

$$i_s = \frac{2FC_{O_2}^b k D_S}{\phi} \quad (8)$$

density that measures the rate of diffusion of the substrate, O_2 , within the electrode coating¹⁹ where F is Faraday's constant, $C_{O_2}^b$

(13) Andrieux, C. P.; Saveant, J.-M. *J. Electroanal. Chem.* **1982**, *131*, 1.

(14) Levich, R. G. “Physicochemical Hydrodynamics”; Prentice-Hall: Englewood Cliffs, NJ, 1962.

(15) Saveant, J.-M.; Vianello, E. *Electrochim. Acta* **1963**, *8*, 905.

(16) Andrieux, C. P.; Merz, A.; Saveant, J.-M.; Tomahogh, R. *J. Am. Chem. Soc.* **1984**, *106*, 1957.

(17) Andrieux, C. P.; Dumas-Bouchlat, J. M.; Saveant, J.-M. *J. Electroanal. Chem.* **1984**, *169*, 9.

(18) Andrieux, C. P.; Saveant, J.-M. *J. Electroanal. Chem.* **1984**, *171*, 65.

Table II. Evaluation of O₂ Penetration Currents, *i_S*, and Ru(NH₃)₆^{3+/2+} Charge Propagation Currents, *i_E*, at Nafion-Coated Electrodes

| $10^7 \Gamma_{\text{Nf}},^a$ mol cm ⁻² | $10^9 \Gamma_{\text{CoP}},^b$ mol cm ⁻² | $i_S,^c$ mA cm ⁻² |
|--|---|---------------------------------|
| 1.5 | 2.5 | 1.10 |
| 1.5 | 3.7 | 1.10 |
| 0.9 | 1.5 | 1.62 |
| $10^7 \Gamma_{\text{Nf}},^a$ mol cm ⁻² | $10^8 \Gamma_{\text{Ru}},^d$ mol cm ⁻² | $i_E,^e$ mA cm ⁻² |
| 1.5 | 1.9 | 1.6 |
| 1.5 | 1.8 | 1.5 |
| 0.9 | 1.2 | 2.8 |

^aSulfonate groups in the Nafion used to coat the electrode. ^bQuantity of CoP present in the Nafion coatings. ^cObtained from the intercepts of Koutecky–Levich plots for the reduction of O₂ at platinum-plated graphite electrodes coated with Nafion–CoP in the absence of Ru(NH₃)₆³⁺ (see text). ^dQuantity of Ru(NH₃)₆³⁺ incorporated in the Nafion coatings. ^eObtained from eq 10.

is the bulk concentration of O₂, κ is the constant governing the partitioning of O₂ between the coating and the solution, D_S is the diffusion coefficient of O₂ within the coating, and ϕ is the thickness of the coating. i_S^* , defined by eq 9, measures the rate of O₂

$$i_S^* = i_S \left(1 - \frac{i_{\text{lim}}}{i_A} \right) \quad (9)$$

diffusion through the coating normalized with respect to the varying concentration of O₂ at the coating/solution interface instead of C_{O_2} ^{b17} where i_{lim} is the measured plateau current density and i_A is the electrode rotation rate-dependent Levich current density¹⁴ corresponding to C_{O_2} ^b.

To measure i_S , the graphite disk electrode was lightly plated with Pt before it was coated with pure Nafion. The reduction of O₂ to H₂O at the resulting electrode is limited by its rate of diffusion through the coating to reach the platinum catalyst sites on the underlying electrode.²⁰ The intercepts of linear Koutecky–Levich plots²¹ of the inverse limiting reduction currents vs. $\omega^{-1/2}$ were equated with $(2i_S)^{-1}$. The factor of 2 accounts for the fact that O₂ is reduced to H₂O at the platinum-plated electrode but only to H₂O₂ by CoP + Ru(NH₃)₆²⁺. Some values of i_S obtained by this procedure are listed in Table II. i_S^* was calculated from the measured i_{lim} values at each rotation rate and O₂ concentration by means of eq 9.

i_E is a measure of the rate at which electrons can be transported across the coating.¹⁹ i_E was evaluated from the slopes, S/I , of linear chronocoulometric charge–(time)^{1/2} plots for the semiinfinite diffusion-limited reduction of the Ru(NH₃)₆³⁺ incorporated in the coatings.²² Measurements were conducted after transfer of the coated electrodes to pure supporting electrolyte solutions. Equation 10 relates the measured slopes and quantities of in-

$$i_E = \frac{\pi(SI)^2}{4FT_{\text{Ru}}} \quad (10)$$

corporated Ru(NH₃)₆³⁺, Γ_{Ru} , to i_E . The measured values of i_E are given in Table II.

$i_{k_1}^*$ is a kinetic current density defined by eq 11 where i_{k_1} is the corresponding kinetic current density normalized with respect

$$i_{k_1}^* = i_{k_1} \left(1 - \frac{i_{\text{lim}}}{i_A} \right) = 2k_1 F C_{\text{O}_2}^b \kappa \Gamma_{\text{CoP}} \left(1 - \frac{i_{\text{lim}}}{i_A} \right) \quad (11)$$

to the bulk concentration of O₂, C_{O_2} ^{b19} Γ_{CoP} is the quantity of cobalt porphyrin in the coating that participates in the catalyzed

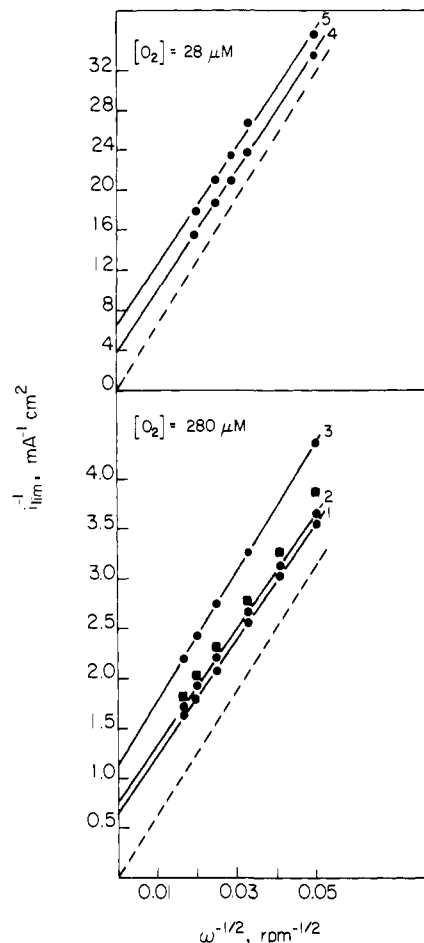


Figure 8. Koutecky–Levich plots ($1/i_{\text{lim}}$ vs. $\omega^{-1/2}$) of the data points from Figure 5B. The dashed lines have the same significance as in Figure 5B. The points shown as solid squares were calculated for conditions corresponding to curve 2 by numerical solution of the governing differential equation (see text).

reduction of O₂, and the other terms have been previously defined. The procedures employed to evaluate i_{k_1} will be described below.

To identify the processes that control the magnitudes of the catalytic O₂ reduction currents and to locate the system on the zone diagram of Figure 7, it is useful to prepare Koutecky–Levich plots of i_{lim}^{-1} vs. $\omega^{-1/2}$ ^{8,15} from the plateau currents of curves such as those shown in Figure 5. Figure 8 contains a set of Koutecky–Levich plots for two concentrations of O₂. The plots are linear and have slopes that match those calculated from the Levich equation^{14,23} for the reduction of O₂ to H₂O₂. In addition, the intercepts of the plots are inversely proportional to the concentration of O₂ in the solution and to the quantity of CoP within the coatings but are independent of the concentration of Ru(NH₃)₆³⁺ in the coatings. The linearity and slopes of the Koutecky–Levich plots as well as their independence of the concentration of Ru(NH₃)₆³⁺ indicate that the catalyst-coated electrode is not operating in any of the zones in Figure 7 that contain an E.¹⁸ That is, the currents are not limited by the rate of transport of electrons across the coating by the Ru(NH₃)₆^{3+/2+} couple. The dependence of the Koutecky–Levich intercepts on the quantity of CoP in the coating indicates that the system is not operating within the zone labeled S.¹⁸ Thus, the Koutecky–Levich plots indicate that the portions of the diagram in Figure 7 that may be relevant for our experiments are those labeled “R1”, “R1 + S”, “SR1”, and, possibly, “General Case”. Since the R1 and SR1 situations are merely limiting versions of the more general R1 + S case,¹⁸ we began by comparing our kinetic data with the behavior expected of a system falling within the R1 + S domain. For such

(19) Andrieux, C. P.; Saveant, J.-M. *J. Electroanal. Chem.* **1982**, *134*, 163.

(20) Wan, G.-X.; Shigehara, K.; Tsuchida, E.; Anson, F. C. *J. Electroanal. Chem.* **1984**, *179*, 239.

(21) Koutecky, J.; Levich, R. G. *Zh. Fiz. Khim.* **1957**, *32*, 1565.

(22) Oyama, N.; Anson, F. C. *J. Electrochem. Soc.* **1980**, *127*, 640.

(23) Bard, A. J.; Faulkner, L. R. “Electrochemical Methods”; Wiley: New York, 1980; p 288.

Table III. Rate Constants for Reaction 1 Evaluated from Rotating Disk Data

| expt | $10^7\Gamma_{\text{Nf}}^a$ mol cm ⁻² | $10^9\Gamma_{\text{Co}}^b$ mol cm ⁻² | [O ₂], mM | $i_{k_1}^c$ mA cm ⁻² | $10^4\kappa k_1^d$ M ⁻¹ s ⁻¹ | $i_{k_1}^e$ mA cm ⁻² |
|------|--|--|--------------------------|------------------------------------|---|------------------------------------|
| 1 | 1.5 | 3.0 | 0.28 | 2.75 | 1.7 | 3.56 |
| 2 | 1.5 | 1.9 | 0.28 | 2.05 | 2.0 | 2.26 |
| 3 | 0.9 | 1.1 | 0.28 | 1.09 | 1.8 | 1.33 |
| 4 | 1.5 | 3.0 | 0.028 | 0.69 | 4.3 | 0.35 |
| 5 | 1.5 | 1.9 | 0.028 | 0.27 | 2.6 | 0.23 |
| 6 | 1.8 | 3.6 | 0.28 | 2.81 | 1.5 | 4.12 |
| 7 | 2.1 | 4.2 | 0.28 | 3.20 | 1.4 | 5.03 |
| | <i>f</i> | | | | 2.2 av | |

^aSulfonate groups in the Nafion used to coat the electrode. ^bQuantity of CoP present in the Nafion coatings as measured coulometrically. ^cCalculated from eq 14. ^dCalculated from eq 11. ^eSelf-consistent set of i_{k_1} values calculated from eq 11 using the average value of κk_1 . ^fIncreasing Γ_{Nf} by much larger factors, e.g., to 15×10^{-7} mol cm⁻², produced smaller values of i_{k_1} than expected on the basis of the data for thinner coatings. This behavior was traced to a decrease in i_E with coating thickness greater than expected.

systems, an analytical expression for the plateau current, i_{lim} can be derived¹⁸

$$i_{\text{lim}} = (i_{k_1}^* i_S^*)^{1/2} \tanh \left[\left(\frac{i_{k_1}^*}{i_S^*} \right)^{1/2} \right] \quad (12)$$

or, in view of the definitions of $i_{k_1}^*$ and i_S^* (eq 9 and 11),

$$(i_{\text{lim}})^{-1} = i_A^{-1} + \left\{ (i_{k_1} i_S)^{1/2} \tanh \left[\left(\frac{i_{k_1}}{i_S} \right)^{1/2} \right] \right\}^{-1} \quad (13)$$

Thus, the "film currents",²⁴ i_F , corresponding to the intercept of the Koutecky-Levich plots in Figure 8 should be given by eq 14.

$$i_F = (i_{k_1} i_S)^{1/2} \tanh \left[\left(\frac{i_{k_1}}{i_S} \right)^{1/2} \right] \quad (14)$$

Equation 14 and the values of i_S in Table II were used to evaluate i_{k_1} , and the product κk_1 was then calculated from eq 11. The resulting values, listed in Table III, are fairly constant, but to be certain that the small variations in κk_1 did not result from the use of eq 14 instead of the equation corresponding to the "general case" in the zone diagram of Figure 7, the complete differential equation governing the behavior of the system²⁵ was solved numerically without approximations by using the values of i_{k_1} in Table III. The resulting calculated plateau currents agreed well with the experimental values. For example, the calculated currents are plotted for comparison with the corresponding experimental values next to curve 2 of Figure 8.

The borders between the various regions of the zone diagram in Figure 7 are actually not as precisely defined as the thin lines on the figure might suggest because the distinction between two neighboring regions becomes somewhat arbitrary near their common boundary.¹⁸ It was therefore useful to locate the experimental data points within the diagram to confirm that they all lie within the R1 + S region. When the average value of κk_1 from Table III was used, a self-consistent set of $i_{k_1}^*$ values was calculated at each electrode rotation rate for the experiments summarized in Table III. The resulting values of $i_{k_1}^*$ were combined with the corresponding values of i_S^* and i_E to locate each data point on the zone diagram in Figure 7. All the data lie well within the R1 + S or SR1 region where the plateau currents are accurately described by eq 13 and 14. Thus, our use of these equations in analyzing the kinetic data obtained with sufficient Ru(NH₃)₆³⁺ in the coatings is consistent with the location of the data points in the zone diagram. Physically, the location of the

data points within the R1 + S and SR1 regions means that the plateau currents are limited by the forward rate of reaction 1. The reaction proceeds throughout the entire coating but with O₂ concentrations that decrease continuously between the coating/solution and electrode/coating interfaces.

The sets of data points move within the zone diagram as the experimental parameters are changed in accord with the vectorial display at the top of the diagram (as they must, of course, because of the way the values of $i_{k_1}^*$ were calculated). This feature of the zone diagram proved quite useful in designing experiments to check that the experimental system matched the kinetic model from which the zone diagram was derived.¹⁸

Variation in the Concentration of Ru(NH₃)₆³⁺. The experiments in Table III were all conducted in the presence of sufficient Ru(NH₃)₆³⁺ to make the measured currents independent of its concentration. If the concentration of Ru(NH₃)₆³⁺ is decreased, one would expect to see an effect on the measured currents not only because i_E decreases but also because the rate of reaction 2 becomes comparable to that of reaction 1 as the ratio $(k_2\Gamma_{\text{Ru}})/(k_{-1}\phi) = (k_2[\text{Ru}(\text{NH}_3)_6^{3+}])/k_{-1}$ approaches unity. Table IV summarizes rotating disk data obtained for three values of Γ_{Ru} and two rotation rates. As anticipated, the measured plateau currents decrease with Γ_{Ru} . Koutecky-Levich plots become nonlinear under these conditions,¹⁸ and it is necessary to solve the general governing differential equation numerically in order to compare the experimental currents with those calculated for a preactivation mechanism with partial control by the rate of reaction 2. (Note that the zone diagram of Figure 7 is also not applicable to plateau currents that exhibit a dependence on the concentration of Ru(NH₃)₆³⁺. To display the behavior of such systems requires a three-dimensional zone diagram¹⁸ that is beyond the intended scope of this work.) The numerical solution of the relevant differential equation²⁵ requires values of i_E , i_S^* , $i_{k_1}^*$, and $\sigma \equiv (k_2[\text{Ru}(\text{NH}_3)_6^{3+}])/k_{-1}$ in the coatings. The three characteristic current densities were available from independent measurements (Tables II and III). In one set of calculations, k_2/k_{-1} was assumed to have the same value as was measured in the experiments in homogeneous solution, namely, $k_2/k_{-1} = 1.7 \times 10^3 \text{ M}^{-1}$, and $[\text{Ru}(\text{NH}_3)_6^{3+}]$ was calculated from the measured values of Γ_{Ru} and an estimate of the coating thickness (0.3 μm for $\Gamma_{\text{Nf}} = 1.5 \times 10^{-7} \text{ mol cm}^{-2}$).^{2c} The resulting values of σ (Table IV) were large enough to yield calculated plateau currents that were independent of Γ_{Ru} in disagreement with the experimental observations (Table IV). We believe that this apparent disagreement arises from the assumption that k_2/k_{-1} will have the same value in the Nafion coatings as in homogeneous solution. The value of k_1/k_{-1} must be small because we encountered no evidence for the formation of significant equilibrium concentrations of the PCO₂ adduct. Since k_1 was measured as $3.6 \times 10^3 \text{ M}^{-1} \text{ s}^{-1}$, it follows that k_{-1} must be larger than, say, 10^4 s^{-1} . If k_{-1} were this large, k_2 measured as $1.7 \times 10^3 k_{-1} \text{ M}^{-1} \text{ s}^{-1}$ in the kinetic experiments in homogeneous solution would be $> 1.7 \times 10^7 \text{ M}^{-1} \text{ s}^{-1}$. This value exceeds the diffusion-limited rate constant, k_d , that can be estimated for Ru(NH₃)₆³⁺ incorporated in Nafion from the Smoluchowski equation²⁶ and its diffusion coefficient as measured by i_E , $k_d \sim 4 \times 10^5 \text{ M}^{-1} \text{ s}^{-1}$.^{2c} Thus, even if the reactivities of Ru(NH₃)₆³⁺ and PCO₂ remained the same in Nafion as in homogeneous solution, one would anticipate that k_2/k_{-1} should be considerably smaller with the reactants incorporated in Nafion. The fifth column and the last column in Table IV show the result of employing a smaller value of k_2/k_{-1} and, therefore, of σ , in calculating the plateau currents. Much better agreement between the experimental and calculated currents results for a value of k_2/k_{-1} that is 500-fold smaller, which does not seem unreasonable in view of the arguments given above that the value of k_2 , a second-order rate constant, is apt to be depressed much more than k_{-1} , a first-order rate constant, is apt to be enhanced by incorporation of the reactants in a Nafion coating. This lower value of k_2/k_{-1} can be used to obtain an (very approximate)

(24) Anson, F. C.; Ohsaka, T.; Saveant, J.-M. *J. Phys. Chem.* **1983**, *87*, 640.

(25) The first "master differential equation" on p 69 of ref 18 was the equation employed in the numerical integration.

(26) von Smoluchowski, M. *Phys. Z.* **1916**, *17*, 557, 585; *Z. Phys. Chem.* **1917**, *92*, 129.

Table IV. Dependence of Plateau Currents for Catalyzed Reduction of O₂ on Γ_{Ru} at Constant Γ_{Co}^a

| $10^9 \Gamma_{Ru}$, mol cm ⁻² | [Ru(NH ₃) ₆ ³⁺], ^b M | i_{lim}^c , mA cm ⁻² | $\omega = 400$ rpm | | $\omega = 3600$ rpm | | |
|--|---|--------------------------------------|--|--|--------------------------------------|--|--|
| | | | i_{calcd}^d , mA cm ⁻² | | i_{calcd} , mA cm ⁻² | | |
| | | | $\sigma = 1.7 \times 10^3$ [Ru(NH ₃) ₆ ³⁺] | $\sigma = 3.3$ [Ru(NH ₃) ₆ ³⁺] | i_{lim}^c , mA cm ⁻² | $\sigma = 1.7 \times 10^3$ [Ru(NH ₃) ₆ ³⁺] | $\sigma = 3.3$ [Ru(NH ₃) ₆ ³⁺] |
| 18 | 0.6 | 0.28 | 0.27 | 0.26 | 0.63 | 0.64 | 0.57 |
| 9 | 0.3 | 0.25 | 0.27 | 0.25 | 0.56 | 0.64 | 0.50 |
| 4.6 | 0.15 | 0.22 | 0.27 | 0.25 | 0.38 | 0.63 | 0.40 |

^a $\Gamma_{Co} = 3.7 \times 10^{-9}$ mol cm⁻² and $\Gamma_{Nf} = 1.5 \times 10^{-7}$ mol cm⁻². ^bConcentration of Ru(NH₃)₆³⁺ in the coating, calculated as Γ_{Ru}/ϕ . For $\Gamma_{Nf} = 1.5 \times 10^{-7}$ mol cm⁻², $\phi = 3 \times 10^{-5}$ cm. ^cMeasured plateau current for reduction of O₂. ^dPlateau current calculated by numerical solution of the governing differential equation for this case.²⁵ For $\Gamma_{Ru} = 18 \times 10^{-9}$ mol cm⁻² the other parameters required were measured as $i_E = 1.5$, $i_S = 1.1$, and $i_k = 3.6$ mA cm⁻². For the other values of Γ_{Ru} , i_E was assumed to be proportional to Γ_{Ru} .

estimate of the equilibrium constant, K_1 , for the formation of the CoP–O₂ adduct in Nafion coatings: if k_2 is taken as 4×10^5 M⁻¹ s⁻¹, i.e., the diffusion-limited rate constant for Ru(NH₃)₆³⁺ in Nafion as calculated from the Smoluchowski equation, and k_2/k_{-1} is set equal to $1/500 \times 1.7 \times 10^3 = 3.4$ M⁻¹, i.e., the value required to obtain the best agreement with the data in Table IV, $k_{-1} = 4 \times 10^5/3.4 = 1.2 \times 10^5$ s⁻¹. Then $\kappa K_1 = \kappa k_1/k_{-1} = 2.2 \times 10^4/1.2 \times 10^5 = 0.2$ M⁻¹. This rough estimate of κK_1 is consistent with the experimental fact that the binding of O₂ by CoP in Nafion is too weak to detect by spectral or electrochemical methods.

Discussion

The average value of κk_1 obtained from the rotating disk measurements, 2.2×10^4 M⁻¹ s⁻¹ (Table III), is about 7 times larger than the value $k_1 = 3.1 \times 10^3$ M⁻¹ s⁻¹ resulting from the kinetic measurements with homogeneous solutions of the reactants. It is possible that $\kappa > 1$ for O₂ at the Nafion–aqueous interface because of the well-known high solubility of O₂ in perfluorinated solvents.²⁷ However, it would be surprising if O₂ were 7 times more soluble in Nafion than in water. Thus, part of the difference between the measured values of κk_1 (within the Nafion coatings) and k_1 (in homogeneous solution) may reflect an increased reactivity of the CoP catalyst incorporated in Nafion. The O₂ faces less competition for axial ligation sites on the cobalt center within the anion-rejecting Nafion coatings, and this could conceivably result in more rapid reduction rates.

Relatively long integration times were required for reduction by Ru(NH₃)₆²⁺ of the last 25–30% of the CoP incorporated in the Nafion coatings, indicating that some of the catalyst resides in portions of the coatings that are less accessible to the Ru(NH₃)₆^{3+/2+} mediator couple than is the majority of the catalyst. Only the more accessible catalyst sites would contribute to the current responses observed for the reduction of O₂ at the effective reaction times at the rotating disk electrode (<1 s). Hence, the actual value of κk_1 within the Nafion coatings may be even larger than the values listed in Table III.

It is also of interest to compare the catalytic behavior of the cobalt porphyrin catalyst immobilized in Nafion coatings with that resulting when it is bound directly to the electrode surface by irreversible adsorption. The latter was the procedure employed successfully in a previous study of the catalysis of O₂ reduction by a cobalt porphyrin that was insoluble in water.²⁸ The water-soluble porphyrin investigated in the present study spontaneously adsorbs on pyrolytic graphite electrodes in amounts of a monolayer or two, but it begins to desorb from the surface within a few minutes after transfer to a pure supporting electrolyte solution. Nevertheless, by working rapidly, it was possible to make rotating disk measurements of O₂ reduction at electrodes on which known quantities of the porphyrin were adsorbed. Linear Koutecky–Levich plots resulted with intercepts that yielded values of k_1 for the adsorbed porphyrin of ca. 10^5 M⁻¹ s⁻¹. This value is somewhat larger than the average value of κk_1 in Table III, probably because all the adsorbed porphyrin participates in the catalysis while only a portion of that incorporated in Nafion is

able to do so (vide supra). However, the Nafion coated electrodes can be adjusted to yield plateau currents no smaller than those obtained with the catalyst adsorbed on the surface in the same solutions, and the catalytic activity is much longer lived with the Nafion coatings. Thus, incorporation of the porphyrin catalyst within the Nafion coatings (along with the necessary mediator) is advantageous with respect to catalyst longevity. Of course, the O₂ reduction proceeds at the more negative potential determined by the formal potential of the mediator redox couple when the catalyst is immobilized within Nafion instead of adsorbed directly on the electrode but this drawback should be avoidable by designing rapidly reacting redox mediators with more positive formal potentials.

Optimization of the Catalyst–Mediator System. It is of general interest to consider how to utilize catalyst–mediator combinations incorporated in polymer coatings in order to obtain the best catalytic efficiencies, defined as the ratio of the measured plateau current, i_{lim} , to the corresponding Levich current, i_A . For a system such as the present one that operates on the right-hand side of the zone diagram in Figure 7 (i.e., under conditions where the currents are independent of the concentration of Ru(NH₃)₆³⁺ in the coating), the experimental variable that can be adjusted to alter the catalytic efficiency is the coating thickness, ϕ . (It is assumed that the concentration of catalyst within the coating material is already at its highest practical value.) For sufficiently thin coatings ($i_S \gg i_{k_1}$), eq 13 simplifies to eq 15 and the catalytic

$$\frac{1}{i_{lim}} = \frac{1}{i_A} + \frac{1}{i_{k_1}} \quad (15)$$

efficiency is given by eq 16. With electrode rotation rates great

$$CAT\ EFF = \frac{i_{k_1}}{i_{k_1} + i_A} \quad (16)$$

enough to avoid depletion of the substrate concentration at the coating/solution interface, $i_A \gg i_{k_1}$ so that $CAT\ EFF = i_{k_1}/i_A$ and, since i_{k_1} is proportional to Γ_{CoP} (eq 11), which increases linearly with the coating thickness, $CAT\ EFF$ increases linearly with ϕ . However, i_S decreases as ϕ increases, and when i_S and i_{k_1} become comparable, the increase in $CAT\ EFF$ with ϕ is smaller and $CAT\ EFF$ ultimately becomes independent of ϕ when $i_{k_1} \gg i_S$ (eq 13). The expected relationship between ϕ and $CAT\ EFF$ is depicted in Figure 9. The portions of the curve corresponding to the relevant domains of the kinetic zone diagram of Figure 7 have been labeled in Figure 9. It is apparent from the figure that the optimum coating thickness, ϕ_{opt} , corresponds to the intersection of the two linear portions of the curve. With $\phi < \phi_{opt}$, higher currents can be obtained by increasing ϕ while with $\phi > \phi_{opt}$ the small additional increases in $CAT\ EFF$ that can be realized require much larger increases in ϕ and, therefore, in consumption of the (often precious) catalyst. Figure 9 may be regarded as a plot of catalyst cost (ϕ) vs. turnover rate ($CAT\ EFF$), and in these terms it seems clear that the point labeled ϕ_{opt} represents the optimum exploitation of the catalytic capabilities of the system. Even in cases where conservation of catalyst is less important than obtaining the maximum possible current densities (i.e., maximum $CAT\ EFF$ values), Figure 9 serves as a useful guide for choosing experimental operating conditions because the maximum possible value of $CAT\ EFF$, corresponding to the SR domain of the zone

(27) Serratrice, G.; Delpuech, J. J.; Diguët, R. *Nouv. J. Chem.* **1982**, *6*, 489.

(28) Durand, R. R., Jr.; Anson, F. C. *J. Electroanal. Chem.* **1982**, *134*, 273.

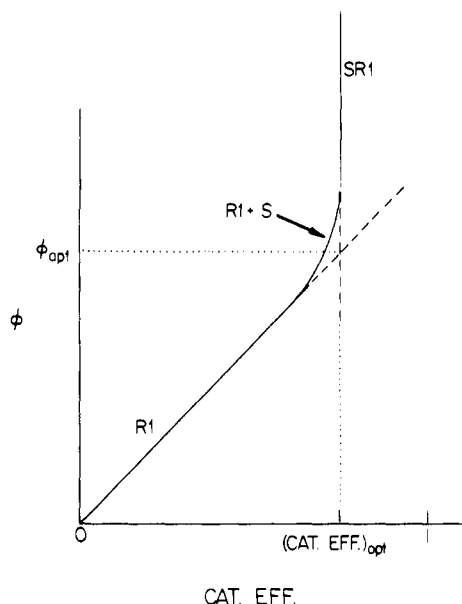


Figure 9. Relationship between catalytic efficiency, $\text{CAT EFF} \equiv i_{\text{lim}}/i_A$, and coating thickness for a catalyst–mediator combination incorporated in polymer coatings on electrodes. The diagram applies to the situation when the current is no longer affected by changes in the concentration of mediator in the coating. The labels on the three segments of the solid curve correspond to the zones in the diagram of Figure 7. The solid line was calculated from the following relevant equations: R1, eq 16 ($i_k \ll i_A$); R1 + S, eq 13; SR1, eq 13 ($i_S \ll i_k$). ϕ_{opt} and $(\text{CAT EFF})_{\text{opt}}$ defined by eq 17 and 18 correspond to the coating thickness at which the catalyst is utilized most efficiently.

diagram, can be obtained with ϕ values only somewhat greater than ϕ_{opt} .

It can be derived from eq 8, 11, and 13 that

$$\phi_{\text{opt}} = \left(\frac{D_S}{k_1[\text{CoP}]_p} \right)^{1/2} \quad (17)$$

where $[\text{CoP}]_p$ is the concentration of cobalt porphyrin in the coating. For the experimental conditions employed in most of the experiments summarized in Table III, the coating thickness was rather close to the optimal value. For example, in experiment 1, ϕ_{opt} calculated from eq 17 is 1.6×10^{-5} cm, and the actual value of ϕ was $\sim 3 \times 10^{-5}$ cm. As expected from Figure 9, small decreases in ϕ produced essentially no changes in the plateau current under these conditions because we were operating on the

steeply rising portions of the curve (i.e., in the R1 + S and SR1 domains) in Figure 9.

The catalytic efficiency obtained when $\phi = \phi_{\text{opt}}$ is given by eq 18 where D_{O_2} is the diffusion coefficient of O_2 in the bulk of the solution and δ , the thickness of the Levich layer^{14,23} at the coating/solution interface, is determined by the electrode rotation rate. Equation 18 leads to the unsurprising conclusion that the

$$(\text{CAT EFF})_{\text{opt}} = \frac{\kappa(D_S k_1 [\text{CoP}]_p)^{1/2}}{\frac{D_{\text{O}_2}}{\delta} + \kappa(D_S k_1 [\text{CoP}]_p)^{1/2}} \quad (18)$$

largest values of $(\text{CAT EFF})_{\text{opt}}$ will result when the coatings are loaded with as much catalyst as they can accommodate. However, increases in $[\text{CoP}]_p$ can result in the system's moving into a new domain of the zone diagram (Figure 7) unless i_S^* and i_E remain much larger than the increasing i_k^* . Thus, it is important to check that the system remains in one of the R1 + S zones (R, R1 + S, SR1) before utilizing eq 17 to calculate the optimal coating thickness or eq 18 to calculate the corresponding optimal catalytic efficiency.

Concluding Remarks

The demonstration that functioning electrode coatings can be fashioned from premixed solutions of soluble Nafion and porphyrin catalysts is an encouraging result; the more so because the catalyst appears to lose none of its reactivity and is longer lived than when adsorbed directly on the electrode surface. That rapidly diffusing, cationic redox couples are readily incorporated by Nafion coatings adds to their appeal because it permits the use of catalysts that are essentially immobile in the coatings, e.g., metalloporphyrins, metalloproteins, etc. The relatively low values of the diffusion coefficient of O_2 within Nafion coatings despite its small size suggests that alternative coating materials that are more highly swollen and may therefore yield larger substrate diffusion rates would be worth developing for use with catalyst–mediator combinations now that the factors which can be varied to obtain optimal catalytic efficiencies have been delineated.

Acknowledgment. This work was supported by the National Science Foundation (Caltech) and the CNRS (Equipe de Recherche Associee 309 "Electrochimie Molculaire") (University of Paris VII). We also acknowledge the North Atlantic Treaty Organization for a travel grant. Discussions with Claude P. Andrieux, Daniel Buttry, and Richard Durand, Jr., were also helpful to us.

Registry No. CoTMPyP, 79346-65-9; $\text{Ru}(\text{NH}_3)_6^{3+}$, 18943-33-4; $\text{Ru}(\text{NH}_3)_6^{2+}$, 19052-44-9; H_2O_2 , 7722-84-1; O_2 , 7782-44-7; graphite, 7782-42-5; Nafion, 39464-59-0.